Enhancement of RF Tag Backscatter Efficiency With Low-Power Reflection Amplifiers

John Kimionis, *Student Member, IEEE*, Apostolos Georgiadis, *Senior Member, IEEE*, Ana Collado, *Senior Member, IEEE*, and Manos M. Tentzeris, *Fellow, IEEE*

***Abstract*—Increasing backscatter tag communication ranges is crucial for the development of low-power long-range wireless sensor networks. A major limitation for increasing the signal-to-noise ratio (SNR) for RF identification tags lies in the fact that tag antennas are terminated with passive loads for modulation, which yields reflection-coefficient values less than unity. Recent work in the field has exploited reflection amplifiers that achieve reflection-coefficient values larger than unity to increase the communication range. However, most of these systems rely on increasing the reflection coefficient at one modulation state only, which is suboptimal. In this paper, an analysis is given for the optimal way to utilize a reflection amplifier and how this compares to suboptimal practices. To demonstrate the concept, a tag is designed that achieves reflection-coefficient values higher than unity for *both* states in the 900–930-MHz band. The two values are antipodal, thus *maximizing* the tag SNR for a given amplifier. The system comprises of an ultra-low-power reflection amplifier with up to 10.2-dB gain and sub-milliwatt power consumption, and a phase-shift modulator that selectively alternates the phase of the backscatter signal between 0° and 180°. The reflection amplifier-phase modulator system is experimentally characterized in terms of gain, power consumption, and backscatter efficiency.**

***Index Terms*—Backscatter radio, increased singal-to-noise ratio (SNR), reflection amplifier, RF identification (RFID) sensors, scattering efficiency.**

I. Introduction

ALTHOUGH the first backscatter radio principles were introduced six decades ago [1], the architecture of most backscatter modulators for RF tags [e.g., RF identification (RFID)] has followed the same pattern; alternating the tag antenna termination between two passive load values to achieve modulation by modifying the reflection of radio waves. Active components (transistors, RF switches, diodes) are introduced to the tag RF front-ends, but are just utilized as mechanisms to switch the antenna load between two states for achieving backscatter modulation. The trend of switching between two load values only has been recently challenged in [2] and [3], but the loads used are still passive, limiting the RF tag scattering efficiency. Scattering efficiency refers to the amount of power a tag can reflect for a given induced power level, in order to perform tag-to-reader communication [4]. Improving the performance of the backscatter link is crucial for achieving a long tag-to-reader communication range. The latter is required for the development of ultra-low-cost and ultra-low-power wireless sensor networks (WSNs) that may utilize backscatter radio instead of active power-hungry radios. Backscatter radio for WSNs has received much attention in the literature [5]–[8], and thus extended ranges constitute a very important design constraint, along with the utilization of energy harvesting, especially from ambient energy sources [9]–[12]. Commercial RFID system architectures, based on all-passive tags and monostatic reader architectures, have been proven to achieve very limited ranges [13], and thus are inappropriate for long-range sensing.

When aiming for long communication ranges of several tens of meters, minimization of the tag bit error rate (BER) at the reader is required, which is associated with the tag-scattered signal's signal-to-noise ratio (SNR). In [14], where the complete backscatter radio signal model is derived by accounting for both communication theory and microwave theory, it can be seen that the tag signal SNR at the reader is

$$\mathrm{SNR} \triangleq \frac{E_b}{N_0} = \frac{P_{\mathrm{tag}}\, T_b}{N_0} \propto |\Delta\Gamma|^2\, T_b. \tag{1}$$

E_b is the bit energy, P_{tag} is the average power of the received tag signal at the reader, T_b is the bit duration, and N_0 is the noise power spectral density. The tag-signal's energy is proportional to $|\Delta\Gamma|^2 \triangleq |\Gamma_1 - \Gamma_0|^2$, where Γ_0, Γ_1 are the complex reflection-coefficient values for the two load values a backscatter tag modulator is using. In [4], it has been stated that maximization of $|\Delta\Gamma|$ is required for improving the RF tag scattering efficiency and minimizing the BER at the reader, regardless of the binary modulation scheme utilized. All modulation schemes can benefit from that efficiency increase; amplitude-shift keying (ASK) waveforms will have higher amplitude values, phase-shift keying (PSK) waveforms will employ signal bases with the maximum possible phase difference, and frequency-shift keying (FSK) waveforms will feature an increased waveform amplitude, positively affecting signal demodulation at the reader. The

Manuscript received July 01, 2014; revised September 30, 2014; accepted October 09, 2014. Date of publication October 29, 2014; date of current version December 02, 2014. This work was supported by the National Science Foundation (NSF), by the Defense Threat Reduction Agency (DTRA), by the Spanish Ministry of Economy and Competitiveness, by FEDER funds under Project TEC2012-39143, by the COST Action IC1301 "Wireless Power Transmission for Sustainable Electronics (WIPE)," and by the Generalitat de Catalunya under Grant 2014 SGR 1551. This paper is an expanded version from the IEEE MTT-S International Microwave Symposium (IMS) 2014, Tampa Bay, FL, USA, June 1–6, 2014.

J. Kimionis and M. M. Tentzeris are with the School of Electrical and Computer Engineering, Georgia Institute of Technology, Atlanta, GA 30332-0250 USA (e-mail: ikimionis@gatech.edu; etentze@ece.gatech.edu).

A. Georgiadis and A. Collado are with the Centre Tecnologic de Telecomunicacions de Catalunya, Castelldefels 08860, Spain (e-mail: ageorgiadis@cttc.es; acollado@cttc.es).

Color versions of one or more of the figures in this paper are available online at http://ieeexplore.ieee.org.

Digital Object Identifier 10.1109/TMTT.2014.2363835

efficient tag demodulation at the reader is translated to an uplink (tag-to-reader) communication range boost, which can be further enhanced by utilizing other-than-monostatic reader architectures [14]. Since RF tags typically utilize passive components for their load modulators, they achieve reflection coefficients Γ_0, Γ_1 with magnitude values less or equal to unity. Thus, all typical load modulators' performance is upper bounded by $|\Delta\Gamma| \leq 2$ with the equality achieved for coefficients with maximum magnitude (unity) and phase difference π or 180° (antipodal points on the Smith chart). This upper bound is limiting backscatter signal SNR maximization and nonconventional tag designs have to be exploited to override this bound. Specifically, to achieve values of $|\Gamma| > 1$, active topologies are required that have a *reflection gain* rather than reflection loss.

A reflection amplifier has been previously proposed for 5.8-GHz RFID tags to amplify the backscattered signal towards the reader by achieving a reflection coefficient higher than unity at one modulation state ($|\Gamma| > 1$) [15]. In that work, the modulation at the amplifier output is achieved by controlling (switching on and off) the amplifier bias; as it will be shown later in this paper, this operation is suboptimal. Moreover that amplifier has been designed without setting strong constraints for the dissipation and requires a few milliamperes for operation. In [16], an active 24-GHz tag was proposed, that achieved up to 15 m by transmitting pseudorandom sequences generated by active antennas with integrated oscillators. However, that system was *radiating* signals towards a reader rather than *reflecting* reader-emitted signals and it required 2.5 V and 26 mA for operation. In [17], a 34.45-GHz tag based on a switched injection-locked oscillator was designed that achieved up to 11.5-m range. That work is more similar to the concept of a system that receives a reader signal, amplifies it, and reflects it, such as in [15] and this paper. It is noted, though, that the front-end incorporates a low-noise amplifier (LNA), power amplifiers (PAs), and complex circuitry for phase locking. The system requires 3 V for operation and its current consumption goes up to 40 $\sim$ 50 mA, which is much higher than the requirement of this work's amplifier.

In this paper, a system architecture is presented that utilizes a reflection amplifier and a phase shifting modulator (Fig. 1, right) to achieve reflection-coefficient amplitudes greater than unity for *both* tag states. The dissipated power of the amplifier is minimized in order to be effectively powered by low-voltage sources such as small batteries, solar cells, or charge tanks. The modulator is designed to perform a 0° or 180° phase shifting on the backscattered signal, thus achieving binary phase shift keying (BPSK) modulation, with antipodal signal bases of the same amplitude, optimizing (maximizing) the $|\Delta\Gamma| > 2$ factor for a given reflection amplifier gain. This maximizes the SNR of the backscattered signal at the reader, significantly enhancing the communication range of an RF tag.

This work is organized as follows. Section II theoretically analyzes the constraints for increased scattering efficiency. Section III describes the design, implementation, and characterization of the reflection amplifier. Section IV describes the design, implementation, and performance of the phase-shifting modulator, and Section V discusses the evaluation of the whole system. Finally, Section VI offers conclusion of this work.

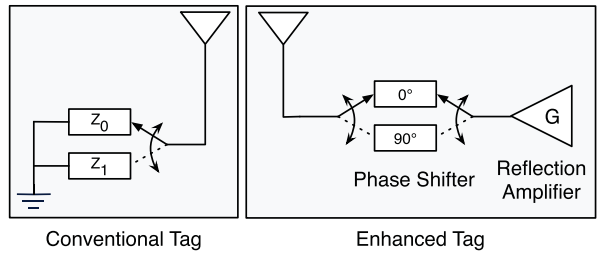

Fig. 1. (*left*) Conventional backscatter RF tag modulator. (*right*) Proposed tag with reflection amplifier and binary phase-shift modulator.

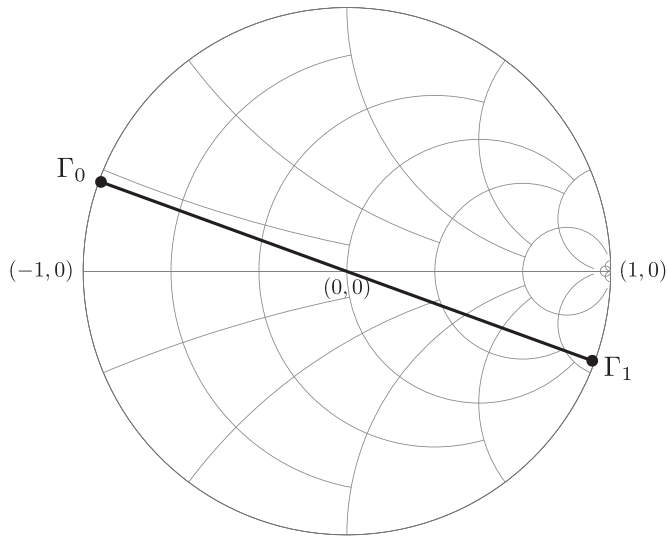

Fig. 2. For a tag with a conventional load modulator, both reflection-coefficient points lie in the Smith chart. In the ideal case, Γ_0 and Γ_1 are antipodal.

II. Increasing Scattering Efficiency

A typical backscatter radio modulator connected to an antenna with input impedance Z_a is switching the antenna termination between two load values Z_0, Z_1 (Fig. 1, left) for bits "0" and "1," respectively [13]. In that way, two different reflection-coefficient values

$$\Gamma_0 = \frac{Z_0 - Z_a^*}{Z_0 + Z_a}, \quad \Gamma_1 = \frac{Z_1 - Z_a^*}{Z_1 + Z_a} \tag{2}$$

are achieved and the amplitude and/or phase of the backscattered signal are altered [4], [18]. The load value selection will affect the reflection-coefficient values and different modulation schemes can be achieved: ASK, PSK, or hybrids. Switching between the two loads multiple times per bit period can yield an FSK signal [14], while switching between M load values can yield high-order modulation schemes, such as M-QAM [2]. The backscattered signal constellation is directly related to the points of Γ_0, Γ_1 on the Smith chart. For example, $\Gamma_0 = -1$ and $\Gamma_1 = 1$ would correspond to BPSK modulation since only the phase of the backscatter signal changes for the two states, while the amplitude remains the same. The same holds for any two antipodal points on the unitary circle (Fig. 2). Notice that for any *passive* load Z_x, the corresponding system reflection coefficient will always have magnitude $|\Gamma_x| \leq 1$. The limitation of $|\Gamma_x| \leq 1$ can be overridden by utilizing a reflection amplifier, which is a

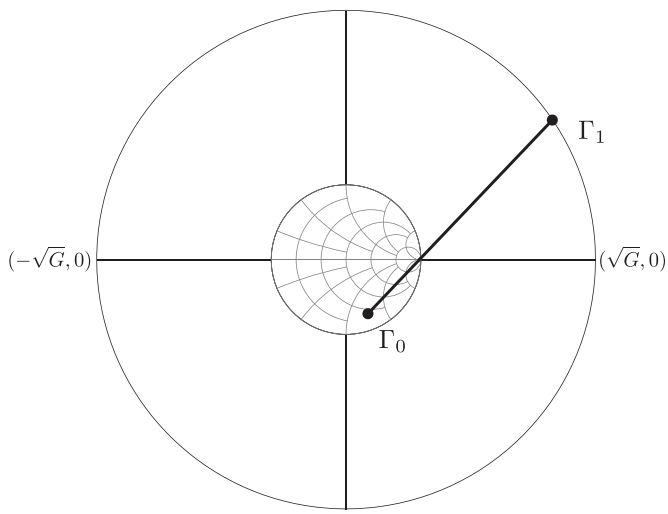

Fig. 3. For a reflection amplifier tag that switches the amplifier on and off, Γ_0 ("off"-state) lies inside the Smith chart, while Γ_1 ("on"-state) lies away from the unitary circle (reflection gain).

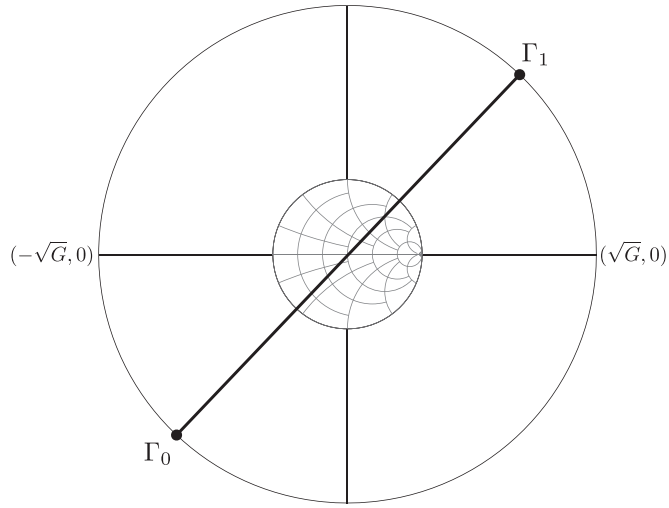

Fig. 4. For a reflection amplifier tag that utilizes a phase-shift modulator, Γ_0 and Γ_1 can both lie far from the unitary circle. Maximum distance between Γ_0 and Γ_1 can be achieved when these are diametrically opposed.

negative resistance oscillator [19], sub-biased in a way that no oscillations occur.

The antipodal load modulator in a classic backscatter radio tag (Fig. 1, left) that maximizes $|\Delta\Gamma|$ switches between two reflection coefficients Γ_0, Γ_1. These reflection coefficients and their difference magnitude are given by

$$\Gamma_0 = 1\, e^{j\theta} \tag{3}$$
$$\Gamma_1 = 1\, e^{j\theta + j\pi} = -1\, e^{j\theta} = -\Gamma_0 \tag{4}$$
$$|\Delta\Gamma| = |e^{j\theta} + e^{j\theta}| = 2 \tag{5}$$

with $\theta \in [0, 2\pi)$. This well-known case is depicted on a Smith chart in Fig. 2, where both coefficients lie on the unitary circle. Notice that passive tags (e.g., RFIDs) that employ antenna-matched harvesters (i.e., the harvester input impedance is $Z_{\rm harv} = Z_a^*$ to maximize power transfer from the antenna to the harvester module) will switch between a matched and an unmatched state, i.e., $\Gamma_0 = 0$ and $\Gamma_1 = 1e^{j\theta}$, achieving a distance $|\Delta\Gamma| = 1$.

Next, consider a system that consists of a reflection amplifier with power gain G directly interfaced to the antenna (as in [15]). The amplifier is switched on and off to achieve ASK modulation. When the amplifier is off, the equivalent circuit seen by the antenna port is a passive load. The system reflection coefficient will have amplitude $B \leq 1$ and arbitrary phase ϕ_0. When on, the amplifier shows a reflection voltage gain $\sqrt{G}$ and applies a phase ϕ_1 to the incoming signal. Thus,

$$\Gamma_0 = B\, e^{j\phi_0} \tag{6}$$
$$\Gamma_1 = \sqrt{G}\, e^{j\phi_1}. \tag{7}$$

Two such reflection-coefficient points are shown in Fig. 3. The reflection-coefficient difference amplitude is

$$|\Delta\Gamma| = |\sqrt{G}\, e^{j\phi_1} - B\, e^{j\phi_0}|. \tag{8}$$

The distance $|\Delta\Gamma|$ is maximized (best case) when $B = 1$ and the line that connects the two points crosses the axis origin $(0, 0)$. This is achieved when $\phi_1 = \phi_0 + \pi$. Then

$$|\Delta\Gamma| = |\sqrt{G}\, e^{j\phi_0 + j\pi} - e^{j\phi_0}| = \sqrt{G} + 1. \tag{9}$$

Similarly, the distance is minimized (worst case) when $B = 1$ and $\phi_1 = \phi_0$. Then

$$|\Delta\Gamma| = |\sqrt{G}\, e^{j\phi_0} - e^{j\phi_0}| = \sqrt{G} - 1. \tag{10}$$

For the proposed system of Fig. 1 (right), consider a reflection amplifier with a gain G that applies an arbitrary phase ϕ_1 to the incoming signal. If the amplifier is constantly on, then its complex S_{11}-parameter is

$$S_{11}^{\rm amp} = \sqrt{G}\, e^{j\phi_1}. \tag{11}$$

Also, consider a two-port phase shifter modulator that can selectively shift the phase of the passing RF signal by 0 or $\pi/2$ by directing it through a delay line, i.e.,

$$S_{21}^{\rm mod} = \begin{cases} 1\, e^{-j\pi/2}, & \text{State 0} \\ 1, & \text{State 1.} \end{cases} \tag{12}$$

The total system input reflection coefficient will then be

$$S_{11}^{\rm system} = S_{21}^{\rm mod}\, S_{11}^{\rm amp}\, S_{21}^{\rm mod} = \begin{cases} -\sqrt{G}\, e^{j\phi_1}, & \text{State 0} \\ \sqrt{G}\, e^{j\phi_1}, & \text{State 1.} \end{cases} \tag{13}$$

Thus, the two reflection coefficients are

$$\Gamma_0 = -\sqrt{G}\, e^{j\phi_1} \tag{14}$$
$$\Gamma_1 = \sqrt{G}\, e^{j\phi_1} = -\Gamma_0 \tag{15}$$

which both have an (equal) amplitude greater than unity, and thus, both lie away from the unitary smith chart circle (Fig. 4). Also, they are diametrically opposed, and the maximum possible reflection-coefficient distance for a given amplifier gain is achieved

$$|\Delta\Gamma| = |\sqrt{G}\, e^{j\phi_1} + \sqrt{G}\, e^{j\phi_1}| = 2\sqrt{G}. \tag{16}$$

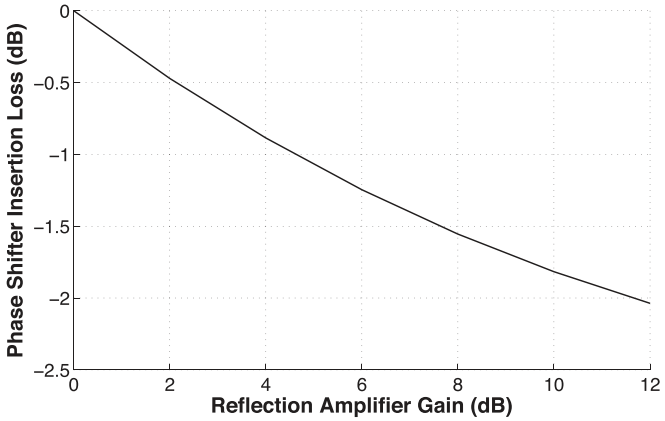

Fig. 5. Maximum acceptable phase-shifter loss for given reflection amplifier gain, to achieve tag SNR gain over conventional tags with load modulators.

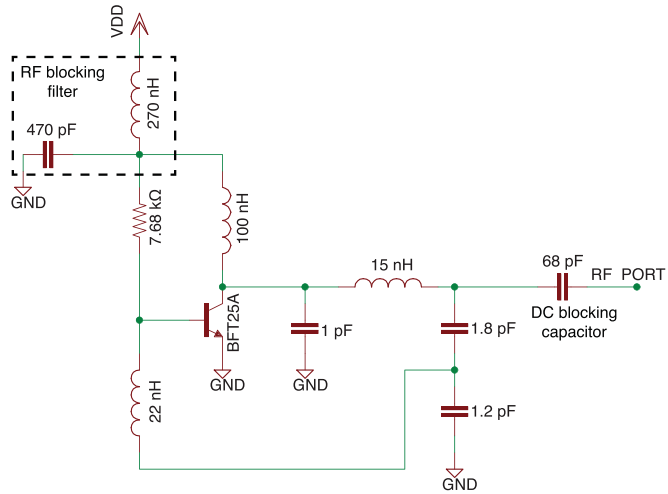

Fig. 6. Reflection amplifier schematic: negative resistance amplifier topology with a common input/output terminal (RF PORT). The amplifier is biased with a low dc voltage to prevent oscillations. An RF blocking filter is utilized at the bias point to prevent RF leakage to the dc supply.

In practice, the phase-shifting modulator will have a power transmission coefficient $0 < T < 1$, and the achievable distance will be

$$|\Delta\Gamma|^{\text{lossy}} = \sqrt{T}\,|\Delta\Gamma|\,\sqrt{T} = 2\,T\sqrt{G}. \tag{17}$$

When the factor T is kept high (low insertion loss), the use of an amplifier-phase-shift modulator system will yield a higher $|\Delta\Gamma|$ than an on–off amplifier system. When compared with the best-case on–off amplifier, a system of the proposed architecture is preferred when

$$2T\sqrt{G} > \sqrt{G} + 1 \Leftrightarrow T > \frac{1}{2} + \frac{1}{2\sqrt{G}} \tag{18}$$

i.e., the insertion loss $10\log_{10} T$ of the phase shifter has to be low. In Fig. 5, the maximum acceptable insertion loss of the phase shifter is plotted versus the amplifier reflection gain. Intuitively, as the amplifier gain increases, the loss level that can be tolerated becomes higher. As an example, for an amplifier reflection gain of 10 dB, the maximum acceptable insertion loss is -1.82 dB.

III. Reflection Amplifier Design

A reflection amplifier is a negative resistance amplifier, which uses a single port as both its input and output terminals. This property leads to compact low-profile circuits, and consequently has been proposed in active antenna implementations for RFID applications, such as in [19] and [20] where 5.25- and 21-GHz tags utilizing reflection amplifiers are proposed. Furthermore, reflection amplifiers have been considered in active reflector circuits used as amplify and forward active antennas in wireless communication scenarios [21]. The negative resistance amplifier concept is attributed to Armstrong [22], [23].

In the case of RFID architectures, a reflection amplifier can be used as a bidirectional amplifier in order to amplify both an incoming signal from the tag antenna towards the tag chip, as well as a reflected signal from the tag chip towards the tag antenna. A bidirectional reflection and transmission amplifier has been proposed in [19], whereas in [24], the combination of two reflection amplifiers and a directional hybrid was used to create a bidirectional amplifier topology used in a 6-GHz Van Atta retro-directive array. In [25], an ultra-high-frequency (UHF) RFID system was proposed that incorporates a coupler and a reflection amplifier circuit. It was shown that provided the amplifier has a minimum gain, the combination of the coupler and amplifier can behave as a bidirectional amplifier, thus leading to improved range of the RFID tag, while minimizing the required number of components and power consumption compared to [15] and [24].

The design of reflection amplifier circuits is similar to oscillator design because the desired amplifier gain is obtained by generating a negative resistance without, however, fulfilling oscillating conditions. Consequently, a challenge in such circuits consists in controlling the stability of the circuit [15], [19], [21], as well as its bandwidth [26].

In this work, emphasis is placed on minimizing the dissipated power and maximizing the efficiency of the reflection amplifier, and for this reason its design was based on a Class-E oscillator topology. A Class-E oscillator is created by introducing appropriate feedback in a Class-E amplifier circuit, which leads to a high dc–RF efficiency. A Class-E power oscillator with 95% efficiency at 2 MHz and with 3-W output power was presented in [27], while a microwave Class-E oscillator with 59% efficiency and 300-mW output power at 5 GHz was demonstrated in [28]. In contrast to typical Class-E oscillator circuit applications, the scenario considered in this work calls for low output power operation while maintaining a high efficiency. In [29], an active antenna oscillator powered by a solar cell was proposed based on the Class-E oscillator topology of [27]. The circuit had a 43% efficiency at 905 MHz for an output power of 2 mW. The device was biased at 1.5 V with a collector current of 3.2 mA. Harmonic-balance simulation was used to ensure the oscillating condition and optimize the output power and efficiency of the circuit. This topology was used as a starting point in order to implement a reflection amplifier. It should be noted that based

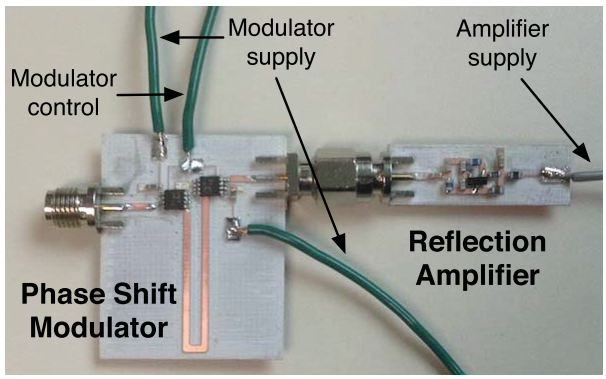

Fig. 7. Fabricated prototypes. (*left*) Phase-shift modulator. (*right*) Reflection amplifier.

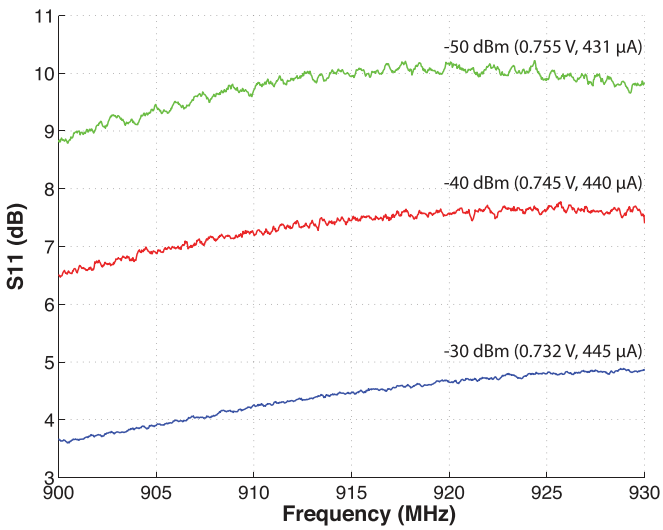

Fig. 8. Reflection amplifier gain measurements for different input power levels and dc bias voltage values.

on the results of [27] and [28], higher efficiency values are considered possible, as well as alternative designs based on devices other than the BFT25A silicon npn transistor used in [29].

The collector bias of the BFT25A device has been reduced until the oscillation is extinguished while maintaining a negative resistance in order to ensure amplifier gain. The circuit schematic of the amplifier with the component values is shown in Fig. 6, while a photograph of the fabricated prototype on a Rogers RO4003C substrate is shown in Fig. 7. Since the amplifier is targeting very long-range applications (order of $50 \sim 100$ m, as in [14]), it has been tuned to maximize its gain at very low input power levels, below -30 dBm. The frequency region of operation is the UHF industrial–scientific–medical (ISM) band of 900–930 MHz.

The reflection gain of the amplifier has been measured with a vector network analyzer (VNA) for several input power levels and bias voltages. The maximum bias voltage used is 0.755 V. In Fig. 8, the obtained reflection gain values (S_{11}) for different bias points and input power levels are shown. It is important to note that the input power levels shown in Fig. 8 correspond to the highest input power that can be injected to the amplifier

TABLE I
REFLECTION AMPLIFIER CONSUMPTION

Input Power (dBm)	Bias Voltage (V)	Current Draw (μA)
-30	0.732	435
-40	0.745	440
-50	0.755	431
no input	0.745	306

for a given bias voltage without starting any oscillation; i.e., if this input power level is exceeded, an oscillation will occur. A maximum gain of 10.2 dB is achieved for an input power level of -50 dBm, when the amplifier is biased at 0.755 V. For lower input power levels, the reflection gain remains on the same level, while the measured current consumption is 431 μA, resulting in 0.325 mW of dissipated power (Table I). This low power level could be supplied by low-cost solar cells, even in low-light illumination conditions. For the same bias voltage and a higher input power level of -40 dBm, the gain will be slightly reduced by ~ 1 dB. During laboratory experiments, it was observed that at a power level of -40 dBm a gain of more than 9 dB can be achieved, but spontaneous interference in the 900–930-MHz band will instantaneously increase the power injected to the amplifier, which starts oscillating. Such interference exists due to nearby RFID readers in the building and other active transmitters in the ISM band. However, in an interference-free environment (e.g., outdoor sensor network deployments, far from domestic infrastructure), a stable operation could be guaranteed. To immune the system from interference and eliminate the probability of starting an oscillation at -40 dBm, the bias voltage has been decreased to 0.745 V.[1] The maximum gain in this case is $\sim$ 7.7 dB and the current consumption is 440 μA. For an input power level of -30 dBm and an even more reduced bias voltage of 0.732 V, the gain reaches 4.9 dB and the consumption is 445 μA. The consumption remains on the sub-milliampere region even for higher input power levels (up to 0 dBm); however, since the amplifier is optimized for low-input power operation, the reflection gain for such power levels decreases significantly. Finally, it is noted that the quiescent current when no RF power is applied at the amplifier's input is 306 μA. Notice that while the input power increases, the amplifier experiences a gain compression. This effect is anticipated and it has been reported in the literature [21].

Some indicative values for frequency, gain values 10–14 dB, bias voltage, and power dissipation are given in Table II for different reflection amplifiers. The amplifiers used in [19] and [20] that are used for tagging applications, similar to the tagging/sensing applications this work's system is targeted, require significantly higher bias voltage of over 2 V for comparable gain values and their power dissipation is on the order of milliwatts. The amplifier in [21] is used for analog relaying and is implemented in 130-nm low-power CMOS technology and achieves an ultra-low-power consumption of 0.120 mW. Although this

[1]One solution to eliminate oscillation is to reset the bias of the amplifier once an oscillation is detected. This can be implemented by sensing the current that the amplifier draws, as the onset of oscillation is marked by an increase in the drain current and dissipation power of the amplifier.

TABLE II
REFLECTION AMPLIFIER COMPARISON

	Frequency	Gain (dB)	Bias Voltage (V)	Power (mW)
this work	915 MHz	10.2	0.755	0.325
[19]	5.25 GHz	13	2.5	2
[20]	21 GHz	14	2.3	209.3
[21]	4 GHz	13	0.8	0.120

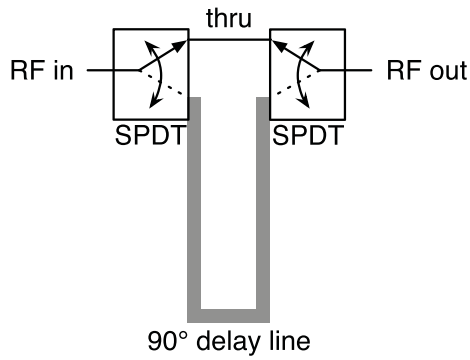

Fig. 9. Delay-line phase-shift modulator block diagram.

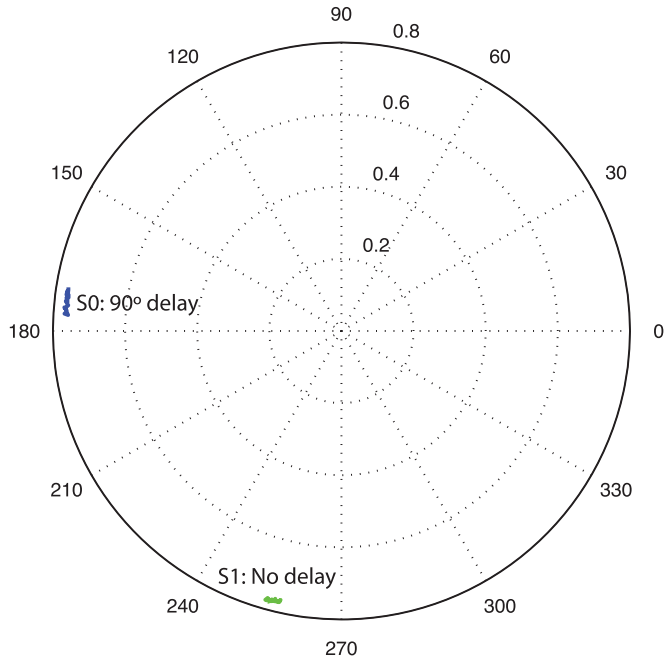

Fig. 10. Transmission coefficient values of the implemented binary phase-shift modulator. State 0: 90° delay. State 1: No delay.

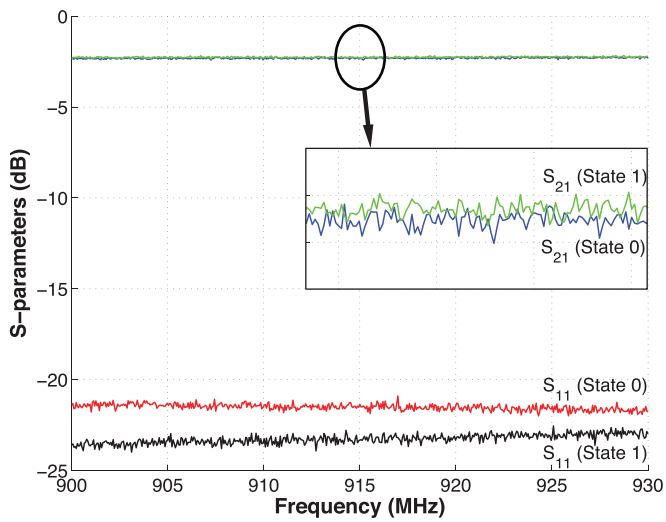

Fig. 11. Measurements of phase-shift modulator insertion loss and return loss for State 0 (90° delay) and State 1 (no delay).

work's amplifier is built using discrete components, its consumption of 0.325 mW is on the same order of magnitude with that of the low-power CMOS circuit.

IV. PHASE-SHIFT MODULATOR DESIGN

A phase-shift modulator is designed as a two-port device that selectively delays the signal by 90° between port 1 and port 2, or passes the signal from port 1 to port 2 with no delay. As expressed mathematically in Section II, in round-trip the reflected signal will be shifted by 180° or 0°, achieving a BPSK modulation.

A delay line of total length $\lambda/4$ is designed in Agilent ADS microwave software and simulated with Agilent Momentum by including the substrate parameters. The line length of $\lambda/4$ at the center frequency of 915 MHz corresponds to a delay of 90°, compared to a zero-length line, which corresponds to 0° (practically, on the order of $3° \sim 5°$). For selecting between the zero-length line and the delay line, two single-pole double-throw (SPDT) switches are utilized (Fig. 9). The SPDT switches will introduce a slight phase change, which does not affect the result since the phase change introduced will be approximately the same for both paths. In that way, the delay-line path will always be 90° shifted compared to the zero-length path.

The phase-shift modulator is implemented on a Rogers RO4003C double copper-clad laminate with dielectric constant $\epsilon_r = 3.55$ and loss tangent $\tan\delta = 0.0021$ (Fig. 7). The substrate thickness of 20 mil helps keeping the microstrip lines in reasonable widths on the order of 40 mil for 915 MHz. Two ADG918 SPDT switches are used, which are operated with microampere current consumption at 1.6 V. The switches have been tested for use with voltages on the order of $1 \sim 1.2$ V with a penalty of slightly higher insertion loss. The SPDTs are controlled by a single pin with a voltage that can be as low as 0.8 V.

The phase-shifter transmission coefficient S_{21} is measured with a VNA to characterize the insertion loss and phase shifting in the two modulator states. In Fig. 10, it can be seen that $|S_{21}| \approx 0.79$, and the phase difference between the two states is $\sim 87°$. The performance of the phase-shift modulator is acceptable, while the transmission coefficient amplitude could be increased by using lower insertion-loss switches. The return loss and insertion loss for both modulator states can be seen in logarithmic scale in Fig. 11. The insertion loss for both states is approximately 2 dB (the two states differ by less than 0.1 dB), while the return loss is better than 21 dB for both states, indicating a good matching. Notice that from Fig. 5, for the reflection amplifier gain of 10.2 dB, the implemented phase-shifter loss on the order of 2 dB is marginally acceptable. Nevertheless, the modulator is sufficient for the purpose of demonstrating the proof-of-concept of a reflection-amplifier

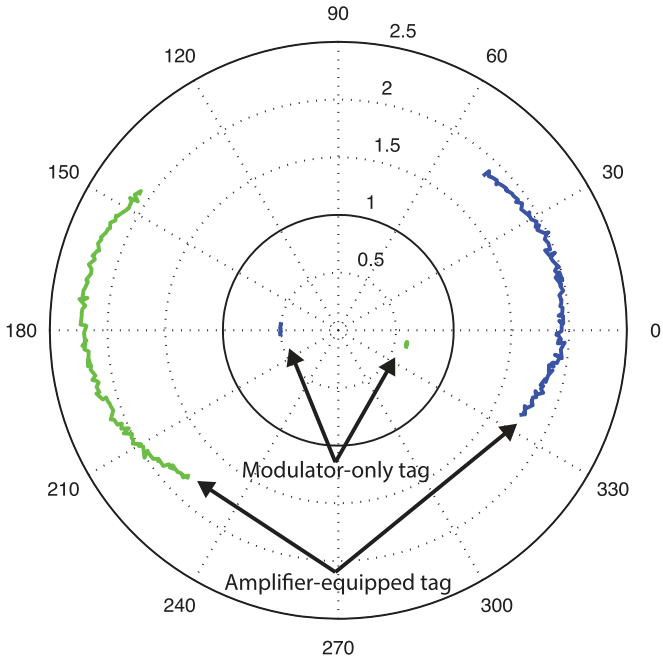

Fig. 12. Measured antipodal reflection-coefficient values (S_{11}) for the two tag modulation states (−40-dBm input power).

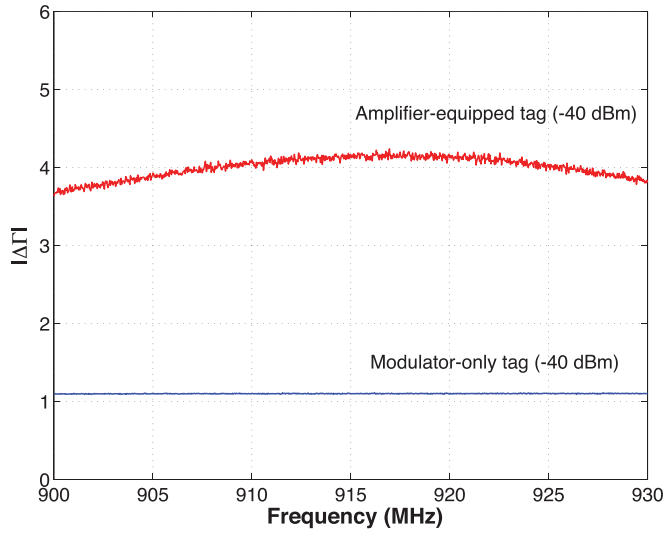

Fig. 13. Comparison of reflection-coefficient distance between the two tag states for a conventional modulator-only tag and an enhanced backscatter efficiency amplifier-equipped tag (−40-dBm input power).

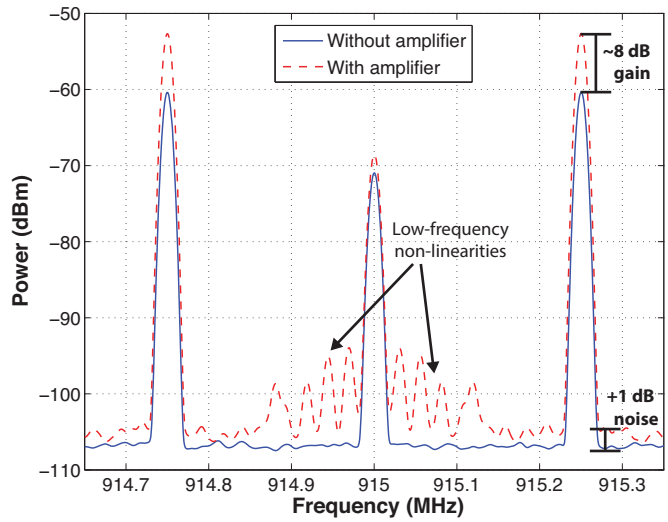

Fig. 14. Measured backscattered spectrum of a conventional tag without a reflection amplifier and an amplifier-equipped tag. Both tags are excited with a 915-MHz CW and continuously switch between two modulation states with a 250-kHz rate, thus backscattering a 250-kHz subcarrier.

phase-shift modulator, and the insertion loss can be minimized by using lower loss SPDT switches, and utilizing a single-board design to eliminate the SMA connector losses.

V. System Characterization

The amplifier phase-shift modulator system is characterized by connecting the two elements (Fig. 7) and measuring the reflection coefficient for the two states. Fig. 12 shows the two reflection coefficients between 900–930 MHz for the amplifier-equipped tag, at a system input power of −40 dBm. At State 0, the reflection coefficient around 915 MHz is approximately $2\angle 15^\circ$, while at State 1, the reflection coefficient is approximately $2.1\angle 197^\circ$. The corresponding phase difference is 182°. The reflection-coefficient amplitude variation across the 900–930-MHz band is on the order of 5%, which is sufficiently low for not affecting the antipodal constellation.

For comparison, a modulator-only tag has been tested, by shorting port 2 of the modulator and measuring the reflection coefficient at the two states. The points can be observed inside the unitary circle, having an amplitude of approximately 0.5 for State 0 and 0.6 for State 1. The phase difference of the two states is approximately 185°, corresponding to a BPSK constellation, with significantly lower SNR than the amplifier-equipped tag constellation.

The reflection-coefficient difference is plotted across the frequency band in Fig. 13 for the amplifier-equipped tag and the modulator-only tag. It can be seen that the amplifier-equipped tag achieves a $|\Delta\Gamma| \approx 4.1$ at 915 MHz, while the modulator-only tag achieves a $|\Delta\Gamma| \approx 1.1$.

Since the tag SNR is proportional to $|\Delta\Gamma|^2$ ([12], [14]), this translates to an SNR gain of the proposed tag over the modulator-only tag of $(4.1/1.1)^2 = 13.89 \rightarrow 11.43$ dB.

A setup consisting of a signal generator, a spectrum analyzer, and a circulator is used to test the backscattering of the implemented tag. The signal generator outputs a continuous wave (CW) at 915 MHz at −40 dBm. The tag is attached to the circulator so that it is excited by the generator CW, and its backscattering is captured by the spectrum analyzer.

Notice that measuring the carrier (central frequency) power level with and without an amplifier is not sufficient for characterization due to: 1) leakage of carrier power towards the spectrum analyzer due to low circulator isolation and 2) the tag reflection at the carrier frequency may have such a phase that will create a destructive addition with the carrier signal from the generator. This can lead to a wrong assessment of the system backscattering efficiency. For that reason, a square waveform is applied to the modulator control pin, switching between the 0°

and 180° states with a rate of 250 kHz. The tag then backscatters a subcarrier 250 kHz away from the carrier (915.25 MHz), whose power level is measured without and with the amplifier. The power level of the subcarrier is directly related to $|\Delta\Gamma|^2$, as shown in the backscatter signal model in [14].

In Fig. 14, the spectra of the two cases can be seen. Notice that the subcarrier power level increases by 8 dB when the amplifier is present compared to the modulator-only case. This gives a proof of the system operation in low input power. The noise floor has been measured to increase by 1 dB on average. This results to a subcarrier SNR increase of $8 - 1 = 7$ dB. An SNR increase of 7 dB can have a significant impact in the tag demodulation by the reader. For example, in [14], it can be seen that for backscatter FSK, an SNR value of 0 dB corresponds to a BER value of 33%. In practice, this tag's information is lost by the reader. However, with a 7-dB increase in SNR, the BER drops down to 6%, which is significantly lower.

Furthermore, notice the low-frequency nonlinearities around the carrier peak, which could cause interference if the tag signal spectrum is close to the carrier. In practice, the frequency region around the carrier is heavily affected by RF clutter due to low-frequency multipath reflections from the surrounding environments and electronics nonlinearities [30]. The nonlinearities introduced by the amplifier will further contribute to the RF clutter, which is a frequency region that should be avoided, due to the increased noise floor. Experiments in [31] have shown that the RF clutter might occupy a bandwidth of up to 100 kHz, and low-SNR tag signals in that frequency region may be completely "hidden" from the reader. Properly selecting high subcarrier values can move the tag signal away from the carrier clutter, and guarantee efficient demodulation of low-SNR tag signals.

The theoretical range increase given an SNR increase of 8 dB can be approximated by using a far-field two-ray path loss model that accounts for a line-of-sight path and a strong reflection from the ground with the formula [32]

$$\mathrm{PL}(d) = G_T + G_R + 20\log_{10}\left(\frac{h_T\, h_R}{d^2}\right) \tag{19}$$

where G_T, G_R are the tag antenna and reader antenna gain values, respectively, h_T, h_R are the heights of the tag and reader antenna placement with respect to ground, and d is the distance between the tag and the reader. Considering a reader that transmits power P_T towards a tag placed at a distance of d_1 meters, the received backscattered power due to round-trip path loss is

$$P_R = P_T + 2\,\mathrm{PL}(d_1). \tag{20}$$

Consider also a tag with increased backscattered power by 8 dB that is placed d_2 m away from the reader, and the reader receives the same backscattered power level

$$P_R = P_T + 8 + 2\,\mathrm{PL}(d_2). \tag{21}$$

It can then be calculated that the tag-to-reader range relation between tag 1 and tag 2 is

$$d_2 \approx 1.26\, d_1 \tag{22}$$

i.e., a range increase of up to 26% can be achieved.

The modulator-amplifier system has been interfaced with a microcontroller unit (MCU) to form a prototype tag and test the BER performance of the system and the range increase in a laboratory environment. The MCU generates a binary FSK waveform and outputs it in a digital pin as a varying frequency square pulse train. The voltage pulses drive the control input of the modulator, and thus the system alternates between Γ_0 and Γ_1 with two different rates F_0 and F_1, respectively. When the system is illuminated by a 915-MHz CW, this results in a backscattered signal spectrum with subcarriers at $\pm F_0$ and $\pm F_1$ (instead of just $\pm F_0$, as in Fig. 14). Both the prototype tag and the SDR reader utilize *omnidirectional* antennas with 3-dBi gain.The backscattered binary FSK signal is captured with a commodity software-defined radio (SDR) and the digitized signal is processed on a host PC. The receiver implemented in software is based on the receiver in [14] and while decoding, it reports BER values of the demodulated backscatter signals. The modulator-only tag (MCU + phase shifter only) and the reader are moved away from each other, until an average BER value of 15% is reported. This corresponds to a distance of 1.39 m in the multipath and interference heavy laboratory environment with a power level of approximately -35 dBm induced at the tag antenna. When the reflection amplifier is interfaced to the tag, the BER drops to 6%, due to the increased backscatter signal SNR. The amplifier-enabled tag and SDR reader are moved away again to achieve a BER value of 15%. The distance in that case is 1.7 m, corresponding to $\sim$ 30-cm range increase. Although this is an indicative example of a 22% increase, the range increase will be different in indoor and outdoor environments with different channel behavior and will vary in heavy interference environments such as buildings with RFID readers, GSM repeaters, etc. However, the laboratory environment example serves as the proof-of-concept for the range increase capabilities of the phase shifter-reflection amplifier architecture.

VI. Conclusion

In this paper, an analysis has been provided for the performance of RF tags that employ reflection amplifiers for enhancing their backscatter efficiency. A new amplifier-equipped tag architecture has been presented that not only increases signal reflection at one modulation state, but *maximizes* the backscatter signal SNR by providing antipodal reflection-coefficient values above unity for *both* modulation states. To demonstrate the tag architecture, a low-power reflection amplifier has been built with sub-milliwatt power consumption and gain values on the order of 10 dB. A phase-shifting network has been designed and implemented that is interfaced at the amplifier's port and achieves antipodal modulation. The latter is optimal in terms of probability of detection at the reader among binary modulation schemes since it maximizes the tag SNR for a given amplifier gain and phase-shifter loss. The increased backscatter signal SNR is crucial for implementing long-range backscatter sensor networks.

This work will be expanded in the future with the design of a tag that includes the phase-shift modulator and reflection amplifier on a single board. In that way, the SMA connectors losses can be eliminated, while the insertion loss of the phase

shifter can be further improved by utilizing low-loss switches. The low-power operation of the amplifier can lead to a design that is powered exclusively by small form-factor solar cells for outdoor deployments. Moreover, an improved amplifier design will increase its dynamic range for operation with a broader span of input power levels. Finally, wireless measurements will be conducted outdoors to assess the practical range increase by accounting for multipath losses in long-range WSN scenarios.

REFERENCES

[1] H. Stockman, "Communication by means of reflected power," *Proc. IRE*, vol. 36, no. 10, pp. 1196–1204, Oct. 1948.

[2] S. Thomas, E. Wheeler, J. Teizer, and M. Reynolds, "Quadrature amplitude modulated backscatter in passive and semipassive UHF RFID systems," *IEEE Trans. Microw. Theory Techn.*, vol. 60, no. 4, pp. 1175–1182, Apr. 2012.

[3] M. S. Trotter, C. R. Valenta, G. A. Koo, B. R. Marshall, and G. D. Durgin, "Multi-antenna techniques for enabling passive RFID tags and sensors at microwave frequencies," in *Proc. IEEE RFID Conf.*, Orlando, FL, USA, Apr. 2012, pp. 1–7.

[4] A. Bletsas, A. G. Dimitriou, and J. N. Sahalos, "Improving backscatter radio tag efficiency," *IEEE Trans. Microw. Theory Techn.*, vol. 58, no. 6, pp. 1502–1509, Jun. 2010.

[5] A. Sample, D. Yeager, P. Powledge, and J. Smith, "Design of a passively-powered, programmable sensing platform for UHF RFID systems," in *Proc. IEEE RFID Conf.*, Grapevine, TX, USA, Mar. 2007, pp. 149–156.

[6] G. Vannucci, A. Bletsas, and D. Leigh, "A software-defined radio system for backscatter sensor networks," *IEEE Trans. Wireless Commun.*, vol. 7, no. 6, pp. 2170–2179, Jun. 2008.

[7] V. Lakafosis, A. Rida, R. Vyas, L. Yang, S. Nikolaou, and M. M. Tentzeris, "Progress towards the first wireless sensor networks consisting of inkjet-printed, paper-based RFID-enabled sensor tags," *Proc. IEEE*, vol. 98, no. 9, pp. 1601–1609, Sep. 2010.

[8] E. Kampianakis, J. Kimionis, K. Tountas, C. Konstantopoulos, E. Koutroulis, and A. Bletsas, "Wireless environmental sensor networking with analog scatter radio & timer principles," *IEEE Sensors J.*, vol. 14, no. 10, pp. 3365–3376, Oct. 2014.

[9] A. P. Sample, J. Braun, A. Parks, and J. Smith, "Photovoltaic enhanced UHF RFID tag antennas for dual purpose energy harvesting," in *IEEE Int. RFID Conf.*, Orlando, FL, USA, Apr. 2011, pp. 146–153.

[10] S. Kim, A. Georgiadis, A. Collado, and M. M. Tentzeris, "An inkjet-printed solar-powered wireless beacon on paper for identification and wireless power transmission applications," *IEEE Trans. Microw. Theory Techn.*, vol. 60, no. 12, pp. 4178–4186, Dec. 2012.

[11] R. J. Vyas, B. B. Cook, Y. Kawahara, and M. M. Tentzeris, "E-WEHP: A batteryless embedded sensor-platform wirelessly powered from ambient digital-TV signals," *IEEE Trans. Microw. Theory Techn.*, vol. 61, no. 6, pp. 2491–2505, Jun. 2013.

[12] J. Kimionis and M. M. Tentzeris, "RF tag front-end design for uncompromised communication and harvesting," in *IEEE Int. RFID Technol. Appl. Conf.*, Tampere, Finland, Sep. 2014, pp. 109–114.

[13] D. M. Dobkin, *The RF in RFID: Passive UHF RFID in Practice*. Newnes, N.S.W., Australia: Elsevier, 2008.

[14] J. Kimionis, A. Bletsas, and J. N. Sahalos, "Increased range bistatic scatter radio," *IEEE Trans. Commun.*, vol. 62, no. 3, pp. 1091–1104, Mar. 2014.

[15] P. Chan and V. Fusco, "Bi-static 5.8GHz RFID range enhancement using retrodirective techniques," in *41st Eur. Microw. Conf.*, Manchester, U.K., Oct. 2011, pp. 976–979.

[16] M. M. Kaleja, P. Heide, and E. M. Biebl, "Imaging RFID system at 24 gigahertz for object localization," in *IEEE MTT-S Int. Microw. Symp. Dig.*, Anaheim, CA, USA, Jun. 1999, pp. 1497–1500.

[17] A. Strobel, C. Carlowitz, R. Wolf, F. Ellinger, and M. Vossiek, "A millimeter-wave low-power active backscatter tag for fmcw radar systems," *IEEE Trans. Microw. Theory Techn.*, vol. 61, no. 5, pp. 1964–1972, May 2013.

[18] F. Fuschini, C. Piersanti, F. Paolazzi, and G. Falciasecca, "Analytical approach to the backscattering from UHF RFID transponder," *IEEE Antennas Wireless Propag. Lett.*, vol. 7, pp. 33–35, 2008.

[19] P. Chan and V. Fusco, "Full duplex reflection amplifier tag," *IET Microw., Antennas, Propag.*, vol. 7, no. 6, pp. 415–420, Apr. 2013.

[20] P. Chan, V. Fusco, and S. Simms, "Microwave reflection amplifier for detection and tagging applications," *IET Microw., Antennas, Propag.*, vol. 2, no. 2, pp. 115–119, Mar. 2008.

[21] J.-F. Bousquet, S. Magierowski, and G. G. Messier, "A 4-GHz active scatterer in 130-nm CMOS for phase sweep amplify-and-forward," *IEEE Trans. Circuits Syst. I, Reg. Papers*, vol. 59, no. 3, pp. 529–540, Mar. 2012.

[22] E. H. Armstrong, "Some recent developments in the audion receiver," *Proc. IRE*, vol. 3, no. 3, pp. 215–238, Sep. 1915.

[23] E. H. Armstrong, "Some recent developments of regenerative circuits," *Proc. IRE*, vol. 10, no. 4, pp. 244–260, Aug. 1922.

[24] S.-J. Chung, S.-M. Chen, and Y.-C. Lee, "A novel bidirectional amplifier with applications in active Van Atta retrodirective arrays," *IEEE Trans. Microw. Theory Techn.*, vol. 51, no. 2, pp. 542–547, Feb. 2003.

[25] J. Kimionis, A. Georgiadis, S. Kim, A. Collado, K. Niotaki, and M. M. Tentzeris, "An enhanced-range RFID tag using an ambient energy powered reflection amplifier," in *IEEE MTT-S Int. Microw. Symp. Dig.*, Tampa, FL, USA, Jun. 2014.

[26] P. Chan and V. Fusco, "An 8- to 12-GHz wideband negative resistance reflection amplifier," *Microw. Opt. Technol. Lett.*, vol. 54, pp. 535–555, Feb. 2012.

[27] J. Ebert and M. Kazimierczuk, "Class E high-efficiency tuned power oscillator," *IEEE J. Solid-State Circuits*, vol. SSC-16, no. 2, pp. 62–66, Apr. 1981.

[28] E. Bryerton, W. Shiroma, and Z. Popović, "A 5-GHz high-efficiency class-E oscillator," *IEEE Microw. Guided Wave Lett.*, vol. 6, no. 12, pp. 441–443, Dec. 1996.

[29] A. Georgiadis and A. Collado, "Solar powered class-E active antenna oscillator for wireless power transmission," in *Proc. IEEE Radio Wireless Symp.*, Austin, TX, USA, Jan. 2013, pp. 40–42.

[30] J. Kimionis, A. Bletsas, and J. N. Sahalos, "Design and implementation of RFID systems with software defined radio," in *6th IEEE Eur. Antennas Propag. Conf.*, Prague, Czech Republic, Mar. 2012, pp. 3464–3468.

[31] E. Kampianakis, J. Kimionis, K. Tountas, and A. Bletsas, "A remotely programmable modular testbed for backscatter sensor network research," in *Proc. 5th Real-World Wireless Sensor Netw. Workshop*, Como Lake, Italy, Sep. 2013, pp. 153–161.

[32] W. C. Jakes, *Microwave Mobile Communications*. Piscataway, NJ, USA: IEEE Press, 1995.

John Kimionis (S'10) received the Diploma degree and M.Sc. degree in electronic and computer engineering from the Technical University of Crete, Crete, Greece, in 2011 and 2013, respectively, and is currently working toward the Ph.D. degree at the Georgia Institute of Technology, Atlanta, GA, USA.

He was with the Telecom Laboratory, University of Crete. He is currently with the School of Electrical and Computer Engineering, Georgia Institute of Technology, as a Research Assistant with the ATHENA Group. His research interests are in the areas of backscatter radio and RFID, wireless sensor networks, software-defined radio for backscatter sensor networks, microwave/RF engineering, telecom modules and algorithms development, and additive manufacturing techniques.

Mr. Kimionis is a member of the IEEE Microwave Theory and Techniques Society (IEEE MTT-S), the IEEE Communications Society, and the IEEE Technical Committee on RFID. He was the recipient of fellowship awards for his undergraduate and graduate studies. He is a Texas Instruments Scholar for his mentoring service for the Opportunity Research Scholars (ORS) program at the Georgia Insititute of Technology. He was the recipient of IEEE student travel grants and the First Best Student Paper Award of the IEEE International Conference on RFID–Technologies and Applications (RFID-TA) 2014, Tampere, Finland, as well as the Second Best Student Paper Award of the IEEE International Conference on RFID–Technologies and Applications (RFID-TA) 2011, Sitges, Barcelona, Spain.

Apostolos Georgiadis (S'94–M'02–SM'08) was born in Thessaloniki, Greece. He received the B.S. degree in physics and M.S. degree in telecommunications from the Aristotle University of Thessaloniki, Thessaloniki, Greece, in 1993 and 1996, respectively, and the Ph.D. degree in electrical engineering from the University of Massachusetts at Amherst, Amherst, MA, USA, in 2002.

In 1995, he spent a semester with Radio Antenna Communications (R.A.C.), Milan Italy. In 2000, he spent three months with Telaxis Communications, South Deerfield, MA, USA. In 2002, he joined Global Communications Devices (GCD), North Andover, MA, USA, where he was a Systems Engineer involved with CMOS transceivers for wireless network applications. In June 2003, he was with Bermai Inc., Minnetonka, MN, USA, where he was an RF/Analog Systems Architect. In 2005, he joined the University of Cantabria, as a Researcher. He is currently a Senior Research Associate and Group Leader with the Microwave Systems and Nanotechnology Department, Centre Tecnològic de Telecomunicacions de Catalunya (CTTC), Barcelona, Spain, where he is involved in the area of communications subsystems, active antennas and antenna arrays, and more recently, with RFID technology and energy harvesting.

Dr. Georgiadis is involved in a number of Technical Program Committees and serves as a reviewer for several journals including the IEEE TRANSACTIONS ON ANTENNAS AND PROPAGATION and the IEEE TRANSACTIONS ON MICROWAVE THEORY AND TECHNIQUES. He was the chairman of COST Action IC0803, RF/Microwave Communication Subsystems for Emerging Wireless Technologies (RFCSET) and the coordinator of Marie Curie Industry–Academia Pathways and Partnerships project Symbiotic Wireless Autonomous Powered system (SWAP). He is a member of the IEEE Microwave Theory and Techniques Society (IEEE MTT-S) TC-24 RFID Technologies (chair 2012–2014) and a member of the IEEE MTT-S TC-26 Wireless Energy Transfer and Conversion. He serves on the Editorial Board of the *Radioengineering Journal* and as an associate editor of the IEEE MICROWAVE AND WIRELESS COMPONENTS LETTERS and *IET Microwaves Antennas and Propagation Journal*. He was the recipient of a 1996 Fulbright Scholarship for graduate studies at the University of Massachusetts at Amherst, the 1997 and 1998 Outstanding Teaching Assistant Award presented by the University of Massachusetts at Amherst, the 1999 and 2000 Eugene M. Isenberg Award presented by the Isenberg School of Management, University of Massachusetts at Amherst, and the 2004 Juan de la Cierva Fellowship presented by the Spanish Ministry of Education and Science. He was the corecipient of the EUCAP 2010 Best Student Paper Award and the ACES 2010 2nd Best Student Paper Award.

Ana Collado (M'08–SM'12) received the M.Sc. and Ph.D. degrees in telecommunications engineering from the University of Cantabria, Santander, Spain, in 2002 and 2007, respectively.

She is currently a Senior Research Associate and the Project Management Coordinator with the Technological Telecommunications Center of Catalonia (CTTC), Barcelona, Spain, where she performs her professional activities. Her professional interests include active antennas, substrate integrated waveguide structures, nonlinear circuit design, and energy harvesting and wireless power transmission (WPT) solutions for self-sustainable and energy efficient systems. She has participated in several national and international research projects. She has coauthored over 70 papers in journals and conferences. Among her activities, she has collaborated in the organization of several international workshops in different countries of the European Union and also a Training School for Ph.D. students. She was a Marie Curie Fellow of the FP7 project Symbiotic Wireless Autonomous Powered System (SWAP).

Dr. Collado serves on the Editorial Board of the *Radioengineering Journal* and is currently an associate editor for *IEEE Microwave Magazine*. She is a member of IEEE MTT-26 Wireless Energy Transfer and Conversion and MTT-24 RFID Technologies.

Manos M. Tentzeris (S'89–M'92–SM'03–F'10) received the Diploma degree in electrical and computer engineering (*magna cum laude*) from the National Technical University of Athens, Athens, Greece, and the M.S. and Ph.D. degrees in electrical engineering and computer science from the University of Michigan, Ann Arbor, MI, USA.

He is currently a Professor with the School of Electrical and Computer Engineering, Georgia Institute of Technology, Atlanta, GA, USA. He has authored or coauthored more than 500 papers in refereed journals and conference proceedings, 5 books, and 19 book chapters. He has helped develop academic programs in highly integrated/multilayer packaging for RF and wireless applications using ceramic and organic flexible materials, paper-based RFIDs and sensors, biosensors, wearable electronics, inkjet-printed electronics, "green" electronics and power scavenging, nanotechnology applications in RF, microwave microelectromechanical systems (MEMs), system-on-package (SOP)-integrated (ultra-wideband (UWB), multiband, millimeter wave, conformal) antennas, and heads the ATHENA research group (20 researchers). He is currently the Head of the GT-ECE Electromagnetics Technical Interest Group. He has served as the Georgia Electronic Design Center Associate Director for RFID/Sensors research (2006–2010) and as the Georgia Institute of Technology National Science Foundation (NSF)-Packaging Research Center Associate Director for RF Research and the RF Alliance Leader (2003–2006). In the summer of 2009, he was a Visiting Professor with the Technical University of Munich, Munich, Germany. In the summer of 2009, he was a Visiting Professor with GTRI-Ireland, Athlone, Ireland. In the summer of 2010, he was a Visiting Professor with LAAS-CNRS, Toulouse, France. He has given more than 100 invited talks to various universities and companies all over the world.

Dr. Tentzeris was the Technical Program Committee (TPC) chair for the 2008 IEEE Microwave Theory and Techniques Society (IEEE MTT-S) International Microwave Symposium (IMS) and the chair of the 2005 IEEE CEM-TD Workshop. He is the vice-chair of the RF Technical Committee (TC16) of the IEEE CPMT Society. He is the founder and chair of the RFID Technical Committee (TC24) of the IEEE MTT-S and the secretary/treasurer of the IEEE C-RFID. He is an associate editor for the IEEE TRANSACTIONS ON MICROWAVE THEORY AND TECHNIQUES, the IEEE TRANSACTIONS ON ADVANCED PACKAGING, and the *International Journal on Antennas and Propagation*. He is a Member of URSI Commission D and the MTT-15 Committee. He is an Associate Member of the European Microwave Association (EuMA). He is a Fellow of the Electromagnetic Academy. He is a member of the Technical Chamber of Greece. Prof. Tentzeris was one of the IEEE MTT-S Distinguished Microwave Lecturers (2010–2012). He was the recipient/corecipient of the 2014 Georgia Institute of Technology Electrical and Computer Engineering Distinguished Faculty Achievement Award, the 2013 IET Microwaves, Antennas and Propagation Premium Award, the 2012 FiDiPro Award (Finland), the iCMG Architecture Award of Excellence, the 2010 IEEE Antennas and Propagation Society Piergiorgio L. E. Uslenghi Letters Prize Paper Award, the 2011 International Workshop on Structural Health Monitoring Best Student Paper Award, the 2010 Georgia Institute of Technology Senior Faculty Outstanding Undergraduate Research Mentor Award, the 2009 IEEE TRANSACTIONS ON COMPONENTS AND PACKAGING TECHNOLOGIES Best Paper Award, the 2009 E. T. S. Walton Award of the Irish Science Foundation, the 2007 IEEE Antennas and Propagation Soceity Symposium Best Student Paper Award, the 2007 IEEE MTT-S IMS Third Best Student Paper Award, the 2007 ISAP 2007 Poster Presentation Award, the 2006 IEEE MTT-S Outstanding Young Engineer Award, the 2006 Asian–Pacific Microwave Conference Award, the 2004 IEEE TRANSACTIONS ON ADVANCED PACKAGING Commendable Paper Award, the 2003 NASA Godfrey "Art" Anzic Collaborative Distinguished Publication Award, the 2003 IBC International Educator of the Year Award, the 2003 IEEE CPMT Outstanding Young Engineer Award, the 2002 International Conference on Microwave and Millimeter-Wave Technology Best Paper Award (Beijing, China), the 2002 Georgia Institute of Technology Electrical and Computer Engineering Outstanding Junior Faculty Award, the 2001 ACES Conference Best Paper Award, the 2000 National Science Foundation (NSF) CAREER Award, and the 1997 Best Paper Award of the International Hybrid Microelectronics and Packaging Society.